Handling the divergence constraints in Maxwell and Vlasov-Maxwell simulations

Martin Campos Pinto, Marie Mounier, Eric Sonnendrücker

Handling the divergence constraints in Maxwell and Vlasov-Maxwell simulations

Martin Campos Pinto[a,b], Marie Mounier[c], Eric Sonnendrücker[d,e]

[a] *CNRS, UMR 7598, Laboratoire Jacques-Louis Lions, F-75005, Paris, France*
[b] *Sorbonne Universités, UPMC Univ Paris 06, UMR 7598, Laboratoire Jacques-Louis Lions, F-75005, Paris, France*
[c] *NUCLETUDES, CS 70117, 91978 Courtaboeuf cedex, France*
[d] *Max-Planck Institute for plasma physics, Boltzmannstr. 2, D-85748 Garching, Germany*
[e] *Mathematics Center, TU Munich, Boltzmannstr. 3, D-85747 Garching, Germany*

Abstract

The aim of this paper is to review and classify the different methods that have been developed to enable stable long time simulations of the Vlasov-Maxwell equations and the Maxwell equations with sources. These methods can be classified in two types: field correction methods and sources correction methods. The field correction methods introduce new unknowns in the equations, for which additional boundary conditions are in some cases non trivial to find. The source correction consists in computing the sources so that they satisfy a discrete continuity equation compatible with a discrete Gauss' law that needs to be defined in accordance with the discretization of the Maxwell propagation operator.

Keywords: Maxwell-Vlasov system, generalised Maxwell equations, discrete continuity equation, Particle in Cell (PIC) method

Corresponding author:
Eric Sonnendrücker
Max-Planck Institute for plasma physics
Boltzmannstr. 2
D-85748 Garching
Germany
email: sonnen@ipp.mpg.de
Phone: +49 89 32992070
Fax: +49 89 32991011

1. Introduction

The collisionless evolution of the distribution of charged particles of a species s is governed by the relativistic Vlasov equation

$$\frac{\partial f_s}{\partial t} + \mathbf{v}_s(\mathbf{p}) \cdot \boldsymbol{\nabla}_{\mathbf{x}} f_s + q_s(\boldsymbol{E} + \mathbf{v}(\mathbf{p}) \times \boldsymbol{B}) \cdot \boldsymbol{\nabla}_{\mathbf{p}} f_s = 0, \tag{1}$$

where $\mathbf{v}_s(\mathbf{p}) = \frac{\mathbf{p}}{m_s \gamma_s}$, the Lorentz factor being defined by $\gamma_s = \sqrt{1 + \frac{\mathbf{p}^2}{m_s c^2}}$ with c the speed of light. Macroscopic quantities relevant to the plasma are obtained as moments in $\mathbf{p}$ of the distribution function f_s for each particle species. In particular the total charge and current densities are defined as

$$\rho = \sum_s q_s \int f_s(t, \mathbf{x}, \mathbf{p}) \, \mathrm{d}\mathbf{p}, \qquad \boldsymbol{J} = \sum_s q_s \int \mathbf{v}_s(\mathbf{p}) f_s(t, \mathbf{x}, \mathbf{p}) \, \mathrm{d}\mathbf{p}. \tag{2}$$

Integrating the Vlasov equation (1) over $\mathbf{p}$ and summing over the species yields the following continuity equation that will play a major role in this paper:

$$\frac{\partial \rho}{\partial t} + \operatorname{div} \boldsymbol{J} = 0. \tag{3}$$

The self-consistent electromagnetic fields $\boldsymbol{E}$ and $\boldsymbol{B}$ appearing in the Vlasov equation satisfy the following Maxwell equations in $(0, T) \times \Omega$,

$$\frac{\partial \boldsymbol{E}}{\partial t} - c^2 \operatorname{curl} \boldsymbol{B} = -\boldsymbol{J}/\varepsilon_0, \tag{4}$$

$$\frac{\partial \boldsymbol{B}}{\partial t} + \operatorname{curl} \boldsymbol{E} = 0, \tag{5}$$

$$\operatorname{div} \boldsymbol{E} = \rho/\varepsilon_0, \tag{6}$$

$$\operatorname{div} \boldsymbol{B} = 0, \tag{7}$$

in addition to initial and boundary conditions. Taking the divergence of the Ampere equation (4) and using the Gauss law (6), we obtain $\frac{\partial \rho}{\partial t} + \operatorname{div} \boldsymbol{J} = 0$ which means that the continuity equation (3) is a compatibility condition for Maxwell's equations, those being ill-posed when the continuity equation is not satisfied. Moreover it can be shown that provided the divergence constraints (6)-(7) are satisfied at the initial time, they remain satisfied for

all times by the solution of Ampere (4) and Faraday (5), which have a unique solution by themselves provided adequate initial and boundary conditions.

At the continuous level, the continuity equation is thus a consequence of the Vlasov equation and all is fine for the Vlasov-Maxwell system. However, for a given discretization of the Vlasov-Maxwell system there is no reason that a discrete continuity equation holds, and that it should be compatible with the discrete Maxwell equations in a certain sense. Even though this is generally the most acute problem in electromagnetic PIC simulations, in some cases problems can appear even without sources: the way in which the Gauss laws (or divergence contraints) are satisfied needs to be compatible with the discrete Ampere and Faraday equations. Handling these compatibility issues is one way to solve the problem. Another is to modify the Maxwell equations, so that they are well posed independently of the sources, by introducing two additional scalar unknowns that can be seen as Lagrange multipliers for the divergence constraints. These should become arbitrarily small when the continuity condition is close to being satisfied.

The aim of this paper is to review the different methods that have been proposed in the literature and classify them in one of the two above categories: using a structure preserving discretization with compatible discrete Gauss laws and continuity equation or using a generalised set of Maxwell equations with additional unknowns that are easier to discretize. Indeed the infinite dimensional kernel of the curl operator and the lack of compactness of the inverse Maxwell operator has made it particularly hard to find good discretization for Maxwell's equations, especially for the eigenvalue problem [4, 5, 9, 14, 26]. Moreover, we will give an overview of classical and new test cases that highlight our problem and the difficulties of the numerical methods.

Although the compatibility problems of discrete Vlasov-Maxwell solvers has been widely discussed in the PIC literature it also exists for grid based discretizations of the Vlasov equations and the same recipes apply there as discussed in [18, 39].

This article is organised as follows: In Section 2 we recall the classical PIC algorithm and the generalised Maxwell equations in Section 3, which can be used to correct the fields. Section 4 is then devoted to presenting the structure preserving methods in which the sources of Maxwell's equations are corrected. This will be discussed in the framework of finite differences, finite elements and discontinuous Galerkin discretizations. Finally the problem and its solutions will be illustrated using different numerical test cases in

Section 5.

2. The Particle in Cell (PIC) method

The principle of a particle method is to approximate the distribution function f solution to the Vlasov equation by a sum of Dirac masses with weights w_k and positions $(\mathbf{x}_k(t), \mathbf{p}_k(t))$ in phase space, $1 \leq k \leq N$. Based on these N macro-particles, the approximated distribution function then writes

$$f_N(t, \mathbf{x}, \mathbf{p}) = \sum_{k=1}^{N} w_k \delta(\mathbf{x} - \mathbf{x}_k(t)) \; \delta(\mathbf{p} - \mathbf{p}_k(t)).$$

Positions $\mathbf{x}_k^0$, momenta $\mathbf{p}_k^0$ and weights w_k are initialised such that $f_N(0, \mathbf{x}, \mathbf{p})$ is an approximation, in some sense, of the initial distribution function $f_0(\mathbf{x}, \mathbf{v})$. The time evolution of the approximation is done by advancing the macro-particles along the characteristics of the Vlasov equation, *i.e.*, by solving the system of differential equations

$$\begin{cases} \dfrac{d\mathbf{x}_k}{dt} = \mathbf{v}(\mathbf{p}_k) \\ \dfrac{d\mathbf{p}_k}{dt} = q(\boldsymbol{E}(\mathbf{x}_k, t) + \mathbf{v}(\mathbf{p}_k) \times \boldsymbol{B}) \end{cases} \quad \text{with} \quad \mathbf{x}_k(0) = \mathbf{x}_k^0, \quad \mathbf{p}_k(0) = \mathbf{p}_k^0.$$

These differential equations are numerically solved by standard ODE solvers like the Runge-Kutta method or preferably a symplectic solver, given the Hamiltonian structure of the equations. We shall not dwell on that as this is not the central theme of the article.

To start the PIC algorithm, the initial distribution function is discretized using a Monte Carlo approach, *i.e.*, the initial phase space positions of the particles are drawn randomly using a pseudo-random or quasi-random number generator according to the probability density associated to f_0, which is just f_0 normalised so that its integral over phase space is one. As f_0 is positive this defines a probability density.

The particle approximation f_N of the distribution function does not naturally give an expression for this function at all points of phase space. Thus for the coupling with the field solver which is defined on the mesh a regularizing step is necessary. To this aim, a standard choice is to use a smooth convolution kernel S which could typically be a Gaussian or preferably in

practice a smooth piecewise polynomial spline function which has the advantage of having a compact support. For a Finite Element discretization of the field, the smoothing kernel is naturally provided by the Finite Element basis functions and no additional smoothing is required.

The sources for Maxwell's equations ρ and $\boldsymbol{J}$ are then naturally defined from the numerical distribution function f_N and the regularisation kernel S, for a particle species of charge q, by

$$\rho_S(t,\mathbf{x}) = q\sum_{k=1}^{N} w_k S(\mathbf{x}-\mathbf{x}_k), \qquad \boldsymbol{J}_S(t,\mathbf{x}) = q\sum_{k=1}^{N} w_k S(\mathbf{x}-\mathbf{x}_k)\mathbf{v}(\mathbf{p}_k). \quad (8)$$

This is obtained by direct discretization. When a structure preserving discretization is needed, in this case a discrete continuity equation, some care must be taken in the full discretization of the current as we shall see later.

With these ingredients the classical PIC loop can be performed at each time step:

1. Compute the fields at the particles positions.
2. Advance the phase space positions of the particles, by numerically integrating the characteristics.
3. Compute the source for Maxwell's equations, namely the current $\boldsymbol{J}$ and in some cases the charge density ρ.
4. Numerically solve Maxwell's equations on a grid.

When a structure preserving method is used, special compatibility conditions between steps 3 and 4 are necessary.

3. Generalised Maxwell's equations: correcting the fields

Even though, provided the divergence constraints are satisfied at the initial condition, they are satisfied at all times for the continuous Maxwell's equations, this is not true for the classical PIC method when only Ampere (4) and Faraday's equations (5) are numerically solved. This has been recognised early in the PIC literature and the first solution proposed by Boris [7], the so-called Boris correction, consists in correcting a posteriori, after each field solve, the electric field $\boldsymbol{E}$ into $\tilde{\boldsymbol{E}} = \boldsymbol{E} + \nabla\varphi$ such that $\nabla\cdot\tilde{\boldsymbol{E}} = \rho/\varepsilon_0$. This yields the Poisson equation

$$-\Delta\varphi = \nabla\cdot\boldsymbol{E} - \frac{\rho}{\varepsilon_0}.$$

In order to avoid a costly Poisson solve, Marder [31] proposed the following correction of the electric field

$$\tilde{\boldsymbol{E}}^{n+1} = \boldsymbol{E}^{n+1} + \Delta t\, \mathbf{grad}(\nu(\nabla \cdot \boldsymbol{E}^n - \rho^n/\varepsilon_0))$$

with ν a diffusion parameter chosen small enough for stability. This method has been further improved by Langdon [28]

$$\tilde{\boldsymbol{E}}^{n+1} = \boldsymbol{E}^{n+1} + \Delta t\, \mathbf{grad}(\nu(\nabla \cdot \boldsymbol{E}^{n+1} - \rho^{n+1}/\varepsilon_0))$$

which can also be seen as one Jacobi iteration for solving the Poisson equation proposed by Boris. A comparison of these methods is performed in [30].

These classical methods can all be interpreted as imposing the divergence constraint on the electric field by using a Lagrange multiplier using the following generalised formulation of Maxwell's equations introduced in [36]

$$\begin{aligned} \partial_t \mathbf{E} - c^2 \operatorname{curl} \mathbf{B} + c^2 \nabla p &= -\frac{\mathbf{J}}{\epsilon_0}, \\ \partial_t \mathbf{B} + \operatorname{curl} \mathbf{E} &= 0, \\ g(p) + \operatorname{div} \mathbf{E} &= \frac{\rho}{\epsilon_0}, \\ \operatorname{div} \mathbf{B} &= 0. \end{aligned}$$

This implies $\frac{\partial g(p)}{\partial t} - c^2 \Delta p = \frac{1}{\epsilon_0}(\frac{\partial \rho}{\partial t} + \operatorname{div} \mathbf{J})$.

A mathematical study of this system has been performed in [2]. The Boris correction corresponds to the case $g = 0$, and the resulting Lagrange multiplier p satisfies a Poisson equation with source $\frac{\partial \rho}{\partial t} + \operatorname{div} \boldsymbol{J}$. The Marder and Langdon corrections are equivalent to two different discretizations of these equations with $g(p) = p$ in which case p satisfies a heat equation transporting the continuity error $\frac{\partial \rho}{\partial t} + \operatorname{div} \boldsymbol{J}$ out of the domain. It then becomes natural to also consider the case $g(p) = \partial_t p$ in which case the Lagrange multiplier satisfies a wave equation and the generalised Maxwell's equations become hyperbolic and even strictly hyperbolic if a Lagrange multiplier is also used for the $\operatorname{div} \boldsymbol{B}$ constraint. This set of generalised Maxwell's equations reads

$$\begin{aligned} \partial_t \mathbf{E} - c^2 \operatorname{curl} \mathbf{B} + c^2 \nabla p &= -\frac{\mathbf{J}}{\epsilon_0}, \\ \partial_t \mathbf{B} + \operatorname{curl} \mathbf{E} + \nabla \tilde{p} &= 0, \\ \frac{\partial p}{\partial t} + \operatorname{div} \mathbf{E} &= \frac{\rho}{\epsilon_0}, \\ \frac{\partial q}{\partial t} + \operatorname{div} \mathbf{B} &= 0. \end{aligned}$$

This is called the hyperbolic correction and was introduced in [35]. The error is transported out of the domain fast enough to avoid accumulation. For this, absorbing boundary conditions are needed.

The idea has also been adapted for imposing the $\operatorname{div} \boldsymbol{B} = 0$ constraint in MHD by Dedner, Kemm, Kröner, Munz, Schnitzer and Wesenberg with considerable success [19].

The hyperbolic generalised Maxwell operator has a compact inverse which can be used to prove the existence and uniqueness of solutions [29], which is not the case for the standard Maxwell's equations. In this case the compactness of the evolution operator is guaranteed for divergence free functions. Hence the Gauss laws enforce that the solution remains in the correct domain. This is what will need to be reproduced at the discrete level. For a generalised formulation such a problem does not exist, which makes it robust for any kind of consistent discretizations. However this comes at some expenses: First two new scalar unknowns are introduced and thus the system to be solved becomes larger. Then these unknowns need boundary conditions which must be found according to the physics problem, which might not always be easy, finding good boundary conditions that dissipate the error is particularly challenging for the hyperbolic correction. Moreover all the generalised Maxwell's equations introduce new non physical propagation speeds in the equations which need to be tuned so as not to distort the physics, which is not always easy. In particular for elliptic and parabolic corrections these wave speeds are infinite. A situation where this is particularly problematic is laser plasma interactions where instabilities can be triggered before the laser hits the plasma due to these spurious wave speeds. This motivates the need of structure preserving algorithms.

4. Structure preserving discretizations: correcting the sources

At the continuous level, we have seen that the Gauss law was preserved thanks to the fact that taking the divergence of the Ampere equation (4) and using the continuity equation (3) yields $\frac{\partial}{\partial t}(\operatorname{div} \boldsymbol{E} - \rho/\varepsilon_0) = 0$. Here we have used in addition to the continuity equation that the divergence of a curl always vanishes, i.e.,

$$\operatorname{div} \mathbf{curl} = 0. \tag{9}$$

The idea of structure preserving discretizations is to get a discrete version of these relations. Thus, we shall look for (semi-) discrete approximations of

the Maxwell equations of the form

$$\begin{cases} \dfrac{\partial \boldsymbol{E}_h}{\partial t} - \mathbf{curl}_h\, B_h = -\dfrac{1}{\varepsilon_0}\boldsymbol{J}_h \\ \dfrac{\partial B_h}{\partial t} + \mathrm{curl}_h\, \boldsymbol{E}_h = 0 \end{cases} \tag{10}$$

with the following properties:

a) the approximate sources must satisfy a discrete continuity equation

$$\frac{\partial \rho_h}{\partial t} + \mathrm{div}_h\, \boldsymbol{J}_h = 0\ ; \tag{11}$$

b) the underlying discrete operators must satisfy a property analogous to that of the continuous ones, namely

$$\mathrm{div}_h\, \mathbf{curl}_h = 0. \tag{12}$$

Clearly, the resulting field will then preserve the corresponding Gauss law,

$$\mathrm{div}_h\, \boldsymbol{E}_h = \frac{\rho_h}{\varepsilon_0} \tag{13}$$

and a similar procedure can be applied for the magnetic field. Numerical methods satisfying the above properties are often said to be *charge conserving* because no spurious charges appear in the longitudinal (i.e., curl-free) part of $\boldsymbol{E}_h$. As we shall see, this program will be sufficient for a large class of methods but will need to be further specified in the general case, see Section 4.3. Note that to simplify the presentation we will restrict ourselves to the skew-symmetric case for the Maxwell equations where

$$\mathbf{curl}_h = (\mathrm{curl}_h)^* \tag{14}$$

which typically corresponds to periodic or metallic boundary conditions.

4.1. Enforcing a "natural" discrete continuity equation

The typical cases where the program outlined above gives satisfactory results is provided by Finite Differences (Yee) schemes and curl-conforming Finite Elements which can be seen as an extension of the former method to higher orders and unstructured meshes. In all these methods, the charge

density is computed in the classical way described previously but the current density is computed differently. Consistent with the physical interpretation, the current is deposited on all cell faces through which a particle passes.

In the scope of Finite Differences the core idea has been introduced by Villasenor and Buneman [42] for the classical cloud in cell method, where particles with hat function shapes (piecewise $\mathbb{Q}_1$ basis functions) are coupled with the Yee scheme [43], and generalised to arbitrary B-spline shape functions by Barthelmé and Parzani [3]. Using a splitting technique, Esirkepov could simplify and accelerate the procedure forcing particle displacements along the axes [23]. In the same spirit Umeda and co-workers [41] introduced a fast procedure for the lowest order scheme. As in this case only the end points of the trajectory are involved in the definition of the charge density, they modify the trajectory between the end points so that the particles cross cell boundaries only through the grid points.

In the framework of the Finite Element method a conservative current deposition scheme has been introduced by Eastwood [21, 22] and generalised in [11] to curl-conforming Finite Elements of arbitrary orders on unstructured meshes. A variant of this algorithm has been proposed recently in [33]. We denote by $\mathcal{T}_h$ a triangulation of the computational domain. Let us specify the construction in the quite general case of so-called *edge*-elements where the approximate electric field is sought in the Nedelec space

$$\mathcal{N}_{p-1}(\mathcal{T}_h;\Omega) := \{\boldsymbol{u} \in H_0(\mathrm{curl};\Omega) : \boldsymbol{u}|_T \in \mathbb{P}^2_{p-1} \oplus \left(\begin{smallmatrix}-y\\ x\end{smallmatrix}\right)\tilde{\mathbb{P}}_{p-1},\ T \in \mathcal{T}_h\} \quad (15)$$

which degrees of freedom involve moments of the tangential traces on the edges of the mesh, see e.g. [37] or [6] for a description in 2d. Based on this space, the standard Finite Element approximation of the time-dependent Maxwell equations consists of finding $\boldsymbol{E}_h(t)$ in the space $\mathcal{N}_{p-1}(\mathcal{T}_h;\Omega)$ and $B_h(t)$ in the fully discontinuous space

$$\mathbb{P}_{p-1}(\mathcal{T}_h) := \{u \in L^2(\Omega) : u|_T \in \mathbb{P}_{p-1},\ T \in \mathcal{T}_h\}, \quad (16)$$

so that the system

$$\begin{cases} \langle \partial_t \boldsymbol{E}_h, \boldsymbol{\varphi}\rangle - \langle B_h, \mathrm{curl}\,\boldsymbol{\varphi}\rangle = -\dfrac{1}{\varepsilon_0}\langle \boldsymbol{J}_h, \boldsymbol{\varphi}\rangle & \boldsymbol{\varphi} \in \mathcal{N}_{p-1}(\mathcal{T}_h;\Omega) \\ \langle \partial_t B_h, \varphi\rangle + \langle \mathrm{curl}\,\boldsymbol{E}_h, \varphi\rangle = 0 & \varphi \in \mathbb{P}_{p-1}(\mathcal{T}_h) \end{cases} \quad (17)$$

holds for all t, where we denote by $\langle \alpha, \beta\rangle$ the L^2 scalar product as well for scalars as for vectors. We note that this method corresponds to defining the

discrete curl operators in (10) by

$$\mathrm{curl}_h : \mathcal{N}_{p-1}(\mathcal{T}_h;\Omega) \ni \boldsymbol{u} \mapsto \mathrm{curl}\,\boldsymbol{u} \in \mathbb{P}_{p-1}(\mathcal{T}_h)$$

and

$$\mathbf{curl}_h := (\mathrm{curl}_h)^* : \mathbb{P}_{p-1}(\mathcal{T}_h) \to \mathcal{N}_{p-1}(\mathcal{T}_h;\Omega),$$

where we recall that the latter amounts to setting $\langle \mathbf{curl}_h\, u, \boldsymbol{v}\rangle := \langle u, \mathrm{curl}_h\, \boldsymbol{v}\rangle$ for all $\boldsymbol{v} \in \mathcal{N}_{p-1}(\mathcal{T}_h;\Omega)$. Given these operators, charge-conserving PIC schemes are based on computing the current density $\boldsymbol{J}_h$ from the particles in such a way that a discrete continuity equation in Finite Element form

$$\langle \partial_t \rho_h, \varphi\rangle + \langle \boldsymbol{J}_h, -\mathbf{grad}\,\varphi\rangle = 0 \qquad \varphi \in \mathcal{L}_p(\mathcal{T}_h;\Omega) \tag{18}$$

holds with continuous test-functions in the ("Lagrange") finite element space

$$\mathcal{L}_p(\mathcal{T}_h;\Omega) := \{u \in H_0^1(\Omega) : u|_T \in \mathbb{P}_p,\ T \in \mathcal{T}_h\}$$

and for some approximation ρ_h of the charge density ρ_S carried by the particles, see (8). It is then easily verified that this method satisfies the program outlined in (10)-(12): First, the finite element continuity equation (18) corresponds to (11) with a discrete divergence operator defined by duality, setting

$$\mathbf{grad}_h : \mathcal{L}_p(\mathcal{T}_h;\Omega) \ni u \mapsto \mathbf{grad}\,u \in \mathcal{N}_{p-1}(\mathcal{T}_h;\Omega)$$

and then

$$\mathrm{div}_h := (-\mathbf{grad}_h)^* : \mathcal{N}_{p-1}(\mathcal{T}_h;\Omega) \to \mathcal{L}_p(\mathcal{T}_h;\Omega). \tag{19}$$

Second, the "structure" relation (12) holds true in this context: indeed for $u \in \mathbb{P}_{p-1}(\mathcal{T}_h)$ we have $\mathrm{div}_h\,\mathbf{curl}_h\,u \in \mathcal{L}_p(\mathcal{T}_h;\Omega)$ and

$$\langle \mathrm{div}_h\,\mathbf{curl}_h\,u, \varphi\rangle = -\langle \mathbf{curl}_h\,u, \mathbf{grad}\,\varphi\rangle = -\langle u, \mathrm{curl}\,\mathbf{grad}\,\varphi\rangle = 0$$

holds for all $\varphi \in \mathcal{L}_p(\mathcal{T}_h;\Omega)$. In particular the resulting scheme will preserve the discrete Gauss law corresponding to (13), namely

$$\langle \boldsymbol{E}_h, -\mathbf{grad}\,\varphi\rangle = \langle \frac{1}{\varepsilon_0}\rho_h, \varphi\rangle \qquad \varphi \in \mathcal{L}_p(\mathcal{T}_h;\Omega) \tag{20}$$

and we note that this is a "natural" discretization of the continuous Gauss law in this Finite Element setting, since it fully characterizes the electrostatic fields of the form $\boldsymbol{E}_h = -\mathbf{grad}\,\phi_h$ with $\phi_h \in \mathcal{L}_p(\mathcal{T}_h;\Omega)$.

In practice the particle current must be deposited in such a way that a fully discrete version of (18) is satisfied, which is essentially done by averaging in time the current (8) carried by the particles. In a leap-frog time scheme for instance, defining

$$\boldsymbol{J}_S^{n+\frac{1}{2}}(\mathbf{x}) := \int_{t_n}^{t_{n+1}} \boldsymbol{J}_S(\mathbf{x},t)\frac{\mathrm{d}t}{\Delta t} = \sum_{k=1}^{N} q w_k \int_{t_n}^{t_{n+1}} S(\mathbf{x}-\mathbf{x}_k(t))\mathbf{v}(\mathbf{p}_k(t))\frac{\mathrm{d}t}{\Delta t} \tag{21}$$

yields [11, Lemma 3.3]

$$\langle \rho_S^{n+1} - \rho_S^n, \varphi\rangle + \Delta t \langle \boldsymbol{J}_S^{n+\frac{1}{2}}, -\mathbf{grad}\,\varphi\rangle = 0 \qquad \varphi \in \mathcal{L}_p(\mathcal{T}_h;\Omega),$$

where the time-discrete charge density is just $\rho_S^n(\mathbf{x}) := \rho_S(t_n,\mathbf{x})$. Thus a fully discrete version of (18) holds with ρ_h^n and $\boldsymbol{J}_h^{n+1/2}$ defined as the orthogonal projections of ρ_S^n and $\boldsymbol{J}_S^{n+1/2}$ on the continuous and curl-conforming finite element spaces, respectively. As for the source vector involved in the matrix form of (a fully discrete version of) the Finite Element Method (17), its entries are the moments of the discrete current $\boldsymbol{J}_h^{n+1/2}$ against the basis functions $\boldsymbol{\varphi}_i$ of $\mathcal{N}_{p-1}(\mathcal{T}_h;\Omega)$. A sketch of the particle trajectory is Figure 1. In the case of point particles ($S=\delta$) their value is

$$\underline{\boldsymbol{J}}_i^{n+\frac{1}{2}} := \langle \boldsymbol{J}_h^{n+\frac{1}{2}}, \boldsymbol{\varphi}_i\rangle = \langle \boldsymbol{J}_S^{n+\frac{1}{2}}, \boldsymbol{\varphi}_i\rangle = \sum_{k=1}^{N} q w_k \int_{t_n}^{t_{n+1}} \mathbf{v}(\mathbf{p}_k(t))\boldsymbol{\varphi}_i(\mathbf{x}_k(t))\frac{\mathrm{d}t}{\Delta t} \tag{22}$$

and for piecewise affine trajectories the function $t \mapsto \mathbf{v}_k^{n+\frac{1}{2}} \cdot \boldsymbol{\varphi}_i(\mathbf{x}_k(t))$ is itself polynomial on every time interval $[\tau, \tau+\Delta\tau] \subset [t_n, t_{n+1}]$ that a particle spends inside a cell. In particular a Gauss formula with enough quadrature points is exact, *i.e.*

$$\int_{\tau}^{\tau+\Delta\tau} \boldsymbol{\varphi}_i(\mathbf{x}_k(t))\frac{\mathrm{d}t}{\Delta t} = \frac{\Delta\tau}{2\Delta t}\sum_{j=1}^{q} \lambda_j\, \boldsymbol{\varphi}_i\big(\mathbf{x}_k(\tau_j)\big)$$

where q needs to be chosen in compliance with the degree of the Finite Element functional space (for instance, with the above choice of Nedelec elements one must take $q \geq \frac{p+1}{2}$ if a Gauss-Legendre quadrature is used).

Remark 1. *The case of Finite Difference schemes can be described with the same arguments, since at lowest order ($p=1$) the above Finite Element*

method applied on a cartesian mesh with the mass lumping procedure of Cohen and Monk [16] is equivalent to the Yee scheme [32]. The above deposition method then coincides with that of Villasenor and Buneman [42].

4.2. Where enforcing a naive discrete continuity equations is not enough

If the above procedure gives satisfactory results when applied to Finite Difference and curl-conforming Finite Element schemes, it is no longer the case when applied to more general solvers such as the Discontinuous Galerkin method [15, 25].

To understand the reasons of this failure and propose a more robust path for designing charge conserving schemes, we may consider as a typical example the DG method with centered fluxes studied in, e.g., [24, 26]. There, the electric and magnetic fields are sought in fully discontinuous spaces such as (16) (thus, in $\mathbb{P}_{p-1}(\mathcal{T}_h)^2$ and $\mathbb{P}_{p-1}(\mathcal{T}_h)$ respectively), as the solutions to

$$\begin{cases} \langle \partial_t \boldsymbol{E}_h, \boldsymbol{\varphi} \rangle - \langle B_h, \widetilde{\mathrm{curl}}_h \boldsymbol{\varphi} \rangle + \displaystyle\sum_{e \in \mathcal{E}_h} \langle \{B_h\}, [\boldsymbol{\varphi}] \rangle_e = -\frac{1}{\varepsilon_0} \langle \boldsymbol{J}_h, \boldsymbol{\varphi} \rangle \\ \langle \partial_t B_h, \varphi \rangle + \langle \boldsymbol{E}_h, \widetilde{\mathbf{curl}}_h \varphi \rangle - \displaystyle\sum_{e \in \mathcal{E}_{h,I}} \langle \{\boldsymbol{E}_h\}, [\varphi] \rangle_e = 0 \end{cases} \tag{23}$$

for all test functions $\boldsymbol{\varphi}$ and φ in $\mathbb{P}_{p-1}(\mathcal{T}_h)^2$ and $\mathbb{P}_{p-1}(\mathcal{T}_h)$. Here the operators

$$\widetilde{\mathrm{curl}}_h \boldsymbol{u} := \sum_{T \in \mathcal{T}_h} \mathrm{curl}\, \boldsymbol{u}|_T \quad \text{and} \quad \widetilde{\mathbf{curl}}_h u := \sum_{T \in \mathcal{T}_h} \mathbf{curl}\, u|_T$$

correspond to "broken curls" in the discontinuous spaces, and standard notations are used for tangential jumps and averages: on interior edges ($e \in \mathcal{E}_{h,I}$) shared by two cells $T_e^{\pm}$ with outward normal unit vectors $\boldsymbol{n}_e^{\pm}$ we let

$$[\boldsymbol{u}]_e := (\boldsymbol{n}_e^- \times \boldsymbol{u}|_{T_e^-} + \boldsymbol{n}_e^+ \times \boldsymbol{u}|_{T_e^+})|_e \quad \text{and} \quad \{\boldsymbol{u}\}_e := \frac{1}{2}(\boldsymbol{u}|_{T_e^-} + \boldsymbol{u}|_{T_e^+}))|_e$$

and on boundary edges ($e \in \mathcal{E}_h \setminus \mathcal{E}_{h,I}$) shared by a single cell T_e we denote

$$[\boldsymbol{u}]_e := (\boldsymbol{n}_e \times \boldsymbol{u}|_{T_e})|_e \quad \text{and} \quad \{\boldsymbol{u}\}_e := (\boldsymbol{u}|_{T_e})|_e.$$

For scalar-valued functions u the definitions are formally the same, keeping in mind that $\boldsymbol{n} \times u$ now corresponds to the vector $(n_y u, -n_x u)^{\mathsf{T}}$.

It is then easily verified that this (semi-discrete) system preserves a discrete Gauss law similar to that of the curl-conforming FEM (17). To do so we define

$$\mathrm{curl}_h^{\mathrm{dg}} : \mathbb{P}_{p-1}(\mathcal{T}_h)^2 \to \mathbb{P}_{p-1}(\mathcal{T}_h) \quad \text{and} \quad \mathbf{curl}_h^{\mathrm{dg}} : \mathbb{P}_{p-1}(\mathcal{T}_h) \to \mathbb{P}_{p-1}(\mathcal{T}_h)^2 \tag{24}$$

by the relations

$$\langle \mathrm{curl}_h^{\mathrm{dg}} \boldsymbol{u}, \varphi \rangle = \langle \boldsymbol{u}, \widetilde{\mathbf{curl}}_h \varphi \rangle - \sum_{e \in \mathcal{E}_{h,I}} \langle \{\boldsymbol{u}\}, [\varphi] \rangle_e, \qquad \varphi \in \mathbb{P}_{p-1}(\mathcal{T}_h) \tag{25}$$

and

$$\langle \mathbf{curl}_h^{\mathrm{dg}} u, \boldsymbol{\varphi} \rangle = \langle u, \widetilde{\mathrm{curl}}_h \boldsymbol{\varphi} \rangle - \sum_{e \in \mathcal{E}_h} \langle \{u\}, [\boldsymbol{\varphi}] \rangle_e, \qquad \boldsymbol{\varphi} \in \mathbb{P}_{p-1}(\mathcal{T}_h)^2, \tag{26}$$

so that (23) corresponds to the abstract system (10) with discrete curls given by (24)-(26). Here a standard computation involving Green formulas yields

$$\mathbf{curl}_h^{\mathrm{dg}} = (\mathrm{curl}_h^{\mathrm{dg}})^* \tag{27}$$

so that the associated evolution operator is skew-symmetric because of the different signs in Ampère and Faraday's laws. Setting then

$$\mathbf{grad}_h^{\mathrm{dg}} : \mathcal{L}_p(\mathcal{T}_h; \Omega) \ni u \mapsto \mathbf{grad}\, u \in \mathbb{P}_{p-1}(\mathcal{T}_h)^2 \tag{28}$$

(which is legitimate since $\mathbf{grad}\, \mathcal{L}_p(\mathcal{T}_h; \Omega) \subset \mathbb{P}_{p-1}(\mathcal{T}_h)^2$) and

$$\mathrm{div}_h^{\mathrm{dg}} := (-\mathbf{grad}_h^{\mathrm{dg}})^* : \mathbb{P}_{p-1}(\mathcal{T}_h)^2 \to \mathcal{L}_p(\mathcal{T}_h; \Omega), \tag{29}$$

we observe that the "structure" relation (12) holds also true in this DG context: for $u \in \mathbb{P}_{p-1}(\mathcal{T}_h)$ we have indeed $\mathrm{div}_h^{\mathrm{dg}} \mathbf{curl}_h^{\mathrm{dg}} u \in \mathcal{L}_p(\mathcal{T}_h; \Omega)$ and

$$\langle \mathrm{div}_h^{\mathrm{dg}} \mathbf{curl}_h^{\mathrm{dg}} u, \varphi \rangle = -\langle \mathbf{curl}_h^{\mathrm{dg}} u, \mathbf{grad}\, \varphi \rangle = -\langle u, \mathrm{curl}_h^{\mathrm{dg}} \mathbf{grad}\, \varphi \rangle = 0$$

for all $\varphi \in \mathcal{L}_p(\mathcal{T}_h; \Omega)$, by using (27) and the fact that $\mathrm{curl}_h^{\mathrm{dg}}$ coincides with the regular curl on the curl-conforming finite element field $\mathbf{grad}\, \varphi$.

In particular, arguing as in Section 4.1 we find that by discretizing the current density as in (22) we preserve the Gauss law $\mathrm{div}_h^{\mathrm{dg}} \boldsymbol{E}_h = \rho_h/\varepsilon_0$, i.e.,

$$\langle \boldsymbol{E}_h, -\mathbf{grad}\, \varphi \rangle = \langle \frac{1}{\varepsilon_0} \rho_h, \varphi \rangle \qquad \varphi \in \mathcal{L}_p(\mathcal{T}_h; \Omega). \tag{30}$$

While this could seem at first glance a quite natural discretization of the continuous Gauss law, one intuitively feels that by taking test functions in the same space as in the conforming case (20) with $\boldsymbol{E}_h$ now belonging to a presumably larger discontinuous space will result in a discrete Gauss law (30) that is *too weak*. And indeed, the corresponding scheme is known to be unstable over large simulations times, as small errors accumulate into large deviations, see e.g. [40] and the numerical results presented in Section 5.

4.3. Enforcing a "strong enough" discrete continuity equation

To answer the question raised in the previous Section – namely: is a given discrete Gauss law strong enough to ensure long-time stability? – we may observe that in the skew-symmetric case (14) where $\operatorname{Im} \mathbf{curl}_h = (\ker \operatorname{curl}_h)^\perp$, the "structure" relation (12) identified above can be restated as

$$(\ker \operatorname{curl}_h)^\perp \subset \ker \operatorname{div}_h \,. \tag{31}$$

However, while this embedding is needed to guarantee that a Gauss law involving the discrete operator div_h will be preserved by the scheme, it does not say anything on the strength of this law. Specifically, the latter should allow to characterize the discrete longitudinal part of the electric fields, i.e., the fields in $\ker \operatorname{curl}_h$, since their temporal growth is not controlled in the evolution equation (10). Thus, we see that in order for the discrete Gauss law to be strong enough to ensure long-time stability, the discrete divergence operator should satisfy

$$\ker \operatorname{curl}_h \subset (\ker \operatorname{div}_h)^\perp$$

as it is the case for the continuous operators. Since this embedding is just the opposite to (31), in the program (10)-(12) the proper "structure" relation should be

$$(\ker \operatorname{curl}_h)^\perp = \ker \operatorname{div}_h \tag{32}$$

and it is not difficult to verify that numerical schemes satifsying these properties are stable over large simulation times.

Note that when applied to the curl-conforming method (17) the above relation amounts to

$$\ker \operatorname{curl}_h = \operatorname{Im} \mathbf{grad}_h$$

which simply expresses the fact that $\mathcal{L}_p(\mathcal{T}_h;\Omega) \xrightarrow{\mathbf{grad}} \mathcal{N}_{p-1}(\mathcal{T}_h;\Omega) \xrightarrow{\operatorname{curl}} \mathbb{P}(\mathcal{T}_h)$ is an exact sequence, a property known for long as essential to the spectral

correctness of the scheme [8, 14, 17, 38, 1]. However (32) does not hold for the discrete operators defined by (25) and (29) in the DG case.

To design charge-conserving current deposition schemes that are consistent with general solvers we are thus left with the following tasks:

i) characterize the kernel of the discrete curl operator defined by the Maxwell solver (10);

ii) find a discrete divergence operator that satisfies the structure relation (32);

iii) define the discrete current $\boldsymbol{J}_h$ seen by the Maxwell solver in such a way that a discrete continuity equation (11) based on this consistent divergence is satisfied.

However recent this approach has already proven successful [12, 34], and when applied to the above DG solver it leads to depositing the current with a "corrected" Galerkin projection, see Section 4.5 below.

4.4. A shortcut: discretizing the sources and the curl in a compatible way

In the case of a pure Maxwell problem where the exact current density $\boldsymbol{J}$ is known, the above analysis still applies but a conceptually shorter path to long-time stability is available. In [13] it was indeed realised that it was possible to characterize approximation operators $\boldsymbol{J} \mapsto \boldsymbol{J}_h$ that provide long-time stability properties to the scheme (10), without any explicit reference to either a discrete continuity equation or a discrete Gauss law (despite the fact that the motivation for such a characterization is driven by a compatibility issue with the Gauss law).

Again, the starting point is to consider the spectral structure of the evolution operator involved in the Maxwell system. At the continuous level first, this is conveniently done in the skew-symmetric (perfect conductor boundaries) and source-free case by rewriting the Ampere and Faraday equations in a compact form

$$\frac{\partial U}{\partial t} - \mathcal{A}U = 0 \qquad \text{with} \qquad U = \begin{pmatrix} \boldsymbol{E} \\ c\boldsymbol{B} \end{pmatrix}, \qquad \mathcal{A} = c \begin{pmatrix} 0 & \mathbf{curl} \\ -(\mathbf{curl})^* & 0 \end{pmatrix}$$

and the associated Gauss laws as

$$\mathcal{D}U = 0 \qquad \text{with} \qquad \mathcal{D} = \begin{pmatrix} (\mathbf{grad})^* & 0 \\ 0 & \mathrm{div} \end{pmatrix}.$$

Using the skew-symmetry of $\mathcal{A}$ we can see that $\operatorname{Im}\mathcal{A} = (\ker\mathcal{A})^\perp \subset \ker\mathcal{D}$, which expresses the fact that the Gauss law is preserved ($\mathcal{D}\mathcal{A} = 0$). But again, more important is the stronger property

$$(\ker\mathcal{A})^\perp = \ker\mathcal{D}.$$

Indeed, using again the skew-symmetry of $\mathcal{A}$ we may decompose

$$L^2 = \ker\mathcal{A} \oplus (\ker\mathcal{A})^\perp \quad \text{with} \quad \begin{cases} \ker\mathcal{A} = \{U : \frac{\partial U}{\partial t} = 0\} \\ (\ker\mathcal{A})^\perp = \operatorname{Span}(\{U : \frac{\partial U}{\partial t} = i\omega U\} : \omega \neq 0) \end{cases}$$

so that the Gauss laws actually mean that the admissible solutions are those which contain no stationary mode. We may now want to reproduce this geometric property at the discrete level. Considering a scheme

$$\frac{\partial U_h}{\partial t} - \mathcal{A}_h U_h = 0$$

where the approximation $\mathcal{A}_h$ of $\mathcal{A}$ satisfies $\mathcal{A}_h = -\mathcal{A}_h^*$ as in the FEM and DG examples shown above, we may state that in the absence of sources, U_h satisfies a "fundamental" discrete Gauss law if it contains no stationary mode with respect to $\mathcal{A}_h$, namely

$$U_h \in (\ker\mathcal{A}_h)^\perp.$$

Now, using the skew-symmetry of $\mathcal{A}_h$ one readily sees that this is in fact equivalent with a property of the initial data, $U_h^0 \in (\ker\mathcal{A}_h)^\perp$. Turning to the case with a source term

$$\frac{\partial U}{\partial t} - \mathcal{A}U = F := \begin{pmatrix} -\frac{1}{\varepsilon_0}\boldsymbol{J} \\ 0 \end{pmatrix},$$

a less obvious step is to find a characterization for the solutions of

$$\frac{\partial U_h}{\partial t} - \mathcal{A}_h U_h = F_h := \Pi_h F \tag{33}$$

that is *compatible* with the above interpretation of the divergence constraints. A minimal requirement is to ask that in the case where the exact solution contains no (continuous) stationary mode, its approximate counterpart should contain no (discrete) stationary mode as well. Thus, we may ask that

$$U \in (\ker\mathcal{A})^\perp \implies U_h \in (\ker\mathcal{A}_h)^\perp$$

and using once again the skew-symmetry of $\mathcal{A}$ and $\mathcal{A}_h$ this can be expressed equivalently on the data, as

$$U^0, F \in (\ker \mathcal{A})^\perp \implies U_h^0, \Pi_h F \in (\ker \mathcal{A}_h)^\perp.$$

Now, since $(\ker \mathcal{A})^\perp = \operatorname{Im} \mathcal{A}$ and $(\ker \mathcal{A}_h)^\perp = \operatorname{Im} \mathcal{A}_h$, the latter condition essentially means that for any continuous field W, there should exist a discrete $W_h \approx W$ such that $\Pi_h \mathcal{A} W = \mathcal{A}_h W_h$. This leads to call *Gauss-compatible* (on a given space $\hat{\mathcal{V}}$ in the domain of $\mathcal{A}$) a scheme of the form (33) for which there exists an approximation operator $\hat{\Pi}_h$ such that

$$\Pi_h \mathcal{A} = \mathcal{A}_h \hat{\Pi}_h \qquad \text{holds on } \ \hat{\mathcal{V}}. \tag{34}$$

Quite surprisingly, this minimal characterization suffices to provide long time stability. Indeed in [13] it is shown that Gauss-compatible schemes satisfy the error estimate

$$\|(U_h - \hat{\Pi}_h U)(t)\| \leq \|U_h^0 - \hat{\Pi}_h U^0\| + \int_0^t \|(\Pi_h - \hat{\Pi}_h)\partial_t U(s)\| \, \mathrm{d}s, \qquad t \geq 0,$$

which implies that U_h cannot deviate from the stationary solutions to (33). And, as was the case for the structure preserving properties identified in Section 4.3, it can be shown that the compatibility condition (34) is satisfied for the curl-conforming finite element methods discussed above and in the Discontinuous Galerkin case suitable projectors can be defined, see [13, 10, 34].

We finally note that condition (34) amounts to saying that the following diagram commutes,

$$\begin{array}{ccc} \hat{\mathcal{V}} & \xrightarrow{\ \mathcal{A}\ } & \mathcal{A}\hat{\mathcal{V}} \\ {\scriptstyle \hat{\Pi}_h}\downarrow & & \downarrow{\scriptstyle \Pi_h} \\ \mathcal{V}_h & \xrightarrow{\ \mathcal{A}_h\ } & \mathcal{V}_h \end{array} \tag{35}$$

where $\mathcal{V}_h$ denotes the discrete space where the solution U_h is sought. This enforces the fundamental property that continuous oscillatory modes are approximated by discrete oscillatory modes and continuous stationary modes by discrete stationary modes, which means more precisely that for $\mathcal{V} \in \ker \mathcal{A}$ we have $\hat{\Pi}_h \mathcal{V} \in \ker \mathcal{A}_h$ and for $\mathcal{V} \in (\ker \mathcal{A})^\perp$ we have $\hat{\Pi}_h \mathcal{V} \in (\ker \mathcal{A}_h)^\perp$.

4.5. Application to DG and DG-PIC schemes: current correction

When applied to a centered DG discretization of the 2d Maxwell system as described in Section 4.2, both the above strategies (be it the "charge-conserving" one described in Section 4.3 or the "Gauss-compatible" one described in Section 4.4) lead to defining the DG current density $\boldsymbol{J}_h \in \mathbb{P}_{p-1}(\mathcal{T}_h)^2$ as a corrected projection of the exact current, of the form

$$\langle \boldsymbol{J}_h, \boldsymbol{\varphi}_i \rangle := \langle \boldsymbol{J}, \mathcal{P}_h \boldsymbol{\varphi}_i \rangle \quad \text{for } \boldsymbol{\varphi}_i \in \mathbb{P}_{p-1}(\mathcal{T}_h)^2. \tag{36}$$

Here $\mathcal{P}_h$ denotes a finite element interpolation on the Nedelec space (15) that is extended to DG fields by local averaging of the edge-based degrees of freedom. For a detailed description we refer to [12, 34] for the cartesian case.

In practice, it is possible to implement this corrected projection in two steps as follows.

- first, perform a standard Galerkin (i.e., orthogonal) projection of the current on some (e.g., DG) space $\tilde{V}_h \supset \mathcal{N}_{p-1}(\mathcal{T}_h; \Omega)$ by computing the products
$$\underline{\tilde{\boldsymbol{J}}}_j := \langle \boldsymbol{J}, \tilde{\boldsymbol{\varphi}}_j \rangle \quad \text{for } \tilde{\boldsymbol{\varphi}}_j \in \tilde{V}_h \ ; \tag{37}$$
- then post-process the resulting values to compute the products of the compatible current $\boldsymbol{J}_h$ defined in (36) with
$$\underline{\boldsymbol{J}}_i := \langle \boldsymbol{J}_h, \boldsymbol{\varphi}_i \rangle = \sum_j \tilde{c}_{i,j} \underline{\tilde{\boldsymbol{J}}}_j \quad \text{for } \boldsymbol{\varphi}_i \in \mathbb{P}_{p-1}(\mathcal{T}_h)^2 \tag{38}$$
where the coefficients $\tilde{c}_{i,j}$ are such that $\mathcal{P}_h \boldsymbol{\varphi}_i = \sum_j \tilde{c}_{i,j} \tilde{\boldsymbol{\varphi}}_j$. This is always possible given that $\tilde{V}_h$ contains the curl-conforming Nedelec space. Moreover it should be emphasized that (38) corresponds to applying a sparse (band) matrix to the array $\underline{\tilde{\boldsymbol{J}}}$, since the projection $\mathcal{P}_h$ is *local*.

For a DG-PIC scheme the same approach can be used to deposit the current from the particles, and the above steps are then to be applied to $\boldsymbol{J} = \boldsymbol{J}_S$. Note that in a fully discrete setting the latter should be defined using time-averages, as described in Section 4.1.

Remark 2. *In order to justify that* (36) *is indeed a Gauss-compatible approximation for the current, one uses the fact that for a well-designed projection operator $\mathcal{P}_h$, the centered DG curl operator defined in* (25) *satisfies*

$$\operatorname{curl}_h^{\mathrm{dg}} = \operatorname{curl} \mathcal{P}_h : \mathbb{P}_{p-1}(\mathcal{T}_h)^2 \to \mathbb{P}_{p-1}(\mathcal{T}_h).$$

see [12, 34]. In the 3d-case things are slightly different, as an additional projection must be added after the curl, see [13].

5. Numerical illustrations

5.1. Maxwell's equations with analytical source (Depeyre-Issautier test case)

As a first test case we consider the Maxwell equations with an analytical current source that has been proposed to study the numerical charge conservation properties in [27, 20] and also considered in [40] to assess the stability of 3d DG solvers with hyperbolic field correction.

Here the problem is posed in a metallic cavity $\Omega = [0,1]^2$, with articifial permittivity ϵ_0 and light speed c equal to one. The given current source is

$$\boldsymbol{J}(t,x,y) = (\cos(t)-1)\begin{pmatrix}\pi\cos(\pi x)+\pi^2 x\sin(\pi y)\\ \pi\cos(\pi y)+\pi^2 y\sin(\pi x)\end{pmatrix} - \cos(t)\begin{pmatrix}x\sin(\pi y)\\ y\sin(\pi x)\end{pmatrix}$$

and an exact solution for this source is

$$\boldsymbol{E}(t,x,y) = \sin(t)\begin{pmatrix}x\sin(\pi y)\\ y\sin(\pi x)\end{pmatrix}$$

and

$$B(t,x,y) = (\cos(t)-1)\big(\pi y\cos(\pi x) - \pi x\cos(\pi y)\big).$$

Note that for this solution the associated charge density reads

$$\rho(t,x,y) = \sin(t)\big(\sin(\pi x)+\sin(\pi y)\big).$$

In Figure 2 we show different results obtained with a centered DG scheme of the form (23) using piecewise $\mathbb{Q}_1$ elements on a 8×8 cartesian mesh and several correction methods. To assess the charge conservation properties of the resulting schemes we plot the time evolution of E_x and the error on the Gauss law $\operatorname{div}\boldsymbol{E}-\rho$ (computed inside every cell where the field is locally $H(\operatorname{div})$). Here we compare the results given by the basic non-corrected scheme where $\boldsymbol{J}_h$ is defined as the standard orthogonal projection of $\boldsymbol{J}$ on the DG space (top row) with those obtained either with a hyperbolic field correction scheme (center row), or with a source correction computed with the technique described in Section 4.5 (bottom row). The advantage of using a correction methods is blatant. Time-wise, we note that while the source correction scheme consumes about the same amount of resources than the basic one, the field correction method requires a significant increase of 33% in cpu time.

5.2. Electromagnetic PIC test cases

5.2.1. The beam test case

In order to test the behaviour of Maxwell solvers coupled with particles we next show simulations of a beam test case which is known to strongly rely on the Gauss law being well satisfied, see for instance [3, 40]. In this test case the domain $\Omega := [0,1]^2 \setminus (B_+ \cup B_-)$ consists of a square of 1 m width minus two disks of radius 0.2 m with respective centers at $(1,1)$ and $(1,0)$, see Figure 3. A bunch of electrons is emitted with current density $500\,\mathrm{Am}^{-2}$ on the left boundary (a metallic cathode) and accelerated by a strong external field $\boldsymbol{E}_{\mathrm{ext}} = -\,\mathbf{grad}\,\phi_{\mathrm{ext}}$ created by the fixed potential maintained between the cathode (where $\phi = 0\,\mathrm{V}$) and on the anode (the two metallic arcs where $\phi = 10^5\,\mathrm{V}$). The right, top and bottom boundaries are absorbing. After a first transient phase the beam propagates towards the right boundary with a steady-state self-consistent field, as depicted in Figure 3.

In Figure 4 we then display the E_x field obtained with three different schemes: in the left panel we show the field computed by the curl-conforming scheme (17) with edge-elements of maximal degree $p = 2$, coupled with the conservative current deposition scheme described in Section 4.1. In the center and right panels we then plot the fields obtained with the centered DG scheme (23) using discontinous elements of degree $p = 1$. Here the center panel corresponds to the uncorrected case where the current density is deposited with a standard method as in Equation (37) alone, which is neither Gauss-compatible nor charge-conserving in the sense specified in Sections 4.3 and 4.4. Finally the right panel shows the field computed with a Gauss-compatible current deposition corresponding to the combined steps (37) and (38). The effectiveness of the latter method is obvious, and is also supported by longer simulations.

5.2.2. 2D matter-photons interaction inside a metallic cavity

We next consider a metallic cavity $\Omega = [-0.5, 0.5] \times [0.5, 0.5]$ whose lower side is hit by a flux of photons during 20 [ns] as depicted in Figure 5. Here the energy of the photons is such that electrons are extracted from the wall, and we simulate the electrons within the cavity. During the emissive phase we inject 200 numerical particles per time step, using an emitting surface of width 600 [mm] and a current density of $1800\,\mathrm{Am}^{-2}$. The initial velocity of the electrons is normal to the wall and corresponds to a kinetic energy of 10 keV.

Before describing the numerical results, we emphasize that there is a property that any qualitatively correct simulation should satisfy. Indeed, since all the emitted electrons are bound to eventually hit and be absorbed by a boundary of the metallic cavity, we observe that all the positive charges created on the cavity surface by the initial loss of these electrons will be eventually neutralized. It follows that there should be no static field at the end of the correct simulations.

In Figures 6 and 7 we compare the results obtained with a centered DG scheme of the form (23) using piecewise $\mathbb{Q}_1$ elements on a 60×60 cartesian mesh and several correction methods, namely the uncorrected scheme (standard projection of the current density carried by the particles), a scheme with hyperbolic field correction and a scheme with source correction as described in Section 4.5.

Here to assess the quality of the simulations we first plot in Figure 6 the E_y field at a point $\mathbf{x} \approx (0, 0.5)$ in the emissive area, for the three versions of the scheme. During the emission time the three curves are almost identical, but after the electrons are emitted the curve corresponding to the uncorrected scheme (in red) does not oscillate around zero, which indicates a physically incorrect behavior as was noticed above. We interpret this phenomenon as being typical of a bad preservation of the Gauss law. Indeed at the continuous level the solutions are only composed of genuinely oscillating fields, at least when all the electrons have been absorbed back by the metallic walls of the cavity. On the other hand, we observe that both correction methods produce the expected behavior, i.e., an field oscillating around zero.

The same phenomenon is visible in Figure 7 where the E_y field is shown in the entire domain together with the numerical particles at 5 ns, 10 ns and 50 ns. The latter snapshot corresponds to a time where the all the electrons have left the domain, however a strong residual field can be seen close to the emitting area. In the corrected DGTD-PIC schemes this residual field is absent which shows the effectiveness of both correction techniques to numerically preserve the charge, be it the hyperbolic field correction or the source correction method.

5.2.3. 2D matter-photons interaction outside a metallic object

In this test case we consider a metallic object whose upper side is hit by a flux of photons during 20 ns, in such a way that the electrons are now extracted *out* of the object and propagate away from it, as depicted Figure 8. The emitting object is now a square of 0.2 m width, and for computational

purposes it is enclosed inside a larger metallic square of 1 m width. Again, the emissive phase is modelled by injecting 200 numerical particles per time step corresponding to a current density of $1800\,\mathrm{Am}^{-2}$, and the initial velocity of the electrons is normal to the wall and corresponds to a kinetic energy of 10 keV.

Unlike in the previous test case where all the emitted electrons would eventually be absorbed back by a metallic surface in contact with the emissive area, a significant fraction of the charge is now expected to leave the simulation domain (or be absorbed by the surrounding metallic surface) without coming back. In particular, a net positive charge should remain on the surface of the emitting metallic object and a non-zero static field is expected to be observed around it.

As above, Figures 9 and 10 allow to compare the results obtained with different versions of a centered DGTD-PIC scheme of the form (23) using piecewise $\mathbb{Q}_1$ elements on a 60×60 cartesian mesh: the uncorrected scheme, the scheme with hyperbolic field correction and the scheme with the source correction described in Section 4.5.

In Figure 9 we show the E_y field at a point $\mathbf{x} \approx (0, 0.1)$ in the emissive area, for the three versions of the scheme. Again, the values are almost identical during the emission time, but after the electrons are emitted the behavior of the three curves is very different. First, we see that the curve corresponding to the uncorrected scheme oscillates around a nonzero value which does not match the expected value (determined with a reference FDTD-PIC code). Moreover this value is not stable, as longer simulations show that it decreases with time: this reflects the bad conservation of charge in the uncorrected scheme. Turning to the hyperbolic correction curve, we observe that it eventually oscillates around zero. As was explained above, this is not qualitatively correct and can be interpreted as a numerical evidence of a bad preservation of the Gauss law. Finally, the curve produced by the source correction method has the expected behavior. Indeed, after 20 ns it oscillates around a constant value of 7.5 V/m which is confirmed by a reference FDTD-PIC scheme.

These findings are confirmed in Figure 10 where the E_y field is shown in the entire domain together with the numerical particles at 5 ns, 10 ns and 50 ns.

Again, notable differences are visible in the latter snapshot which corresponds to a time where the electrons have left the computational domain: in the uncorrected scheme (top row) a strong unphysical field is present close to

the emissive area, in the field corrected scheme (center row) the residual field is close to zero which does not match with the presence of positive charges on the inner metallic object, and finally the source correction scheme (bottom row) computes a qualitatively correct field.

We note that the reason why the field correction method does not give charge-conserving results for this test case lies in the fact that the boundary conditions are not properly taken into account in the propagation of the corrected field. To do so it would be necessary to represent the surface charge density on the emitting object, which requires additional steps in the discretization process that are not straighfoward. In particular, this test-case reflects the advantage of the source correction method for DGTD-PIC codes, as it overcomes the need of properly representing the surface charge density.

6. Conclusion

In the numerical approximation of Maxwell's equations an adequate discretization of the divergence constraints (or involutions) plays a major role in getting accurate and stable solutions over long simulation times. This problem becomes even more important in the presence of sources. Because these constraints put additional requirements on the discrete solutions there are essentially too options: either relax them by adding additional degrees of freedom, or make them compatible with the discretization. The former choice corresponds to field correction methods and we have described the latter as source correction methods. In this paper we set the framework for both techniques, reviewed different implementations and also provided some numerical illustrations highlighting the problem and its solutions.

Acknowledgement:. This work was performed in part during Marie Mounier's PhD thesis in the Nuclétudes company, which was supported by DGA .

[1] D.N. Arnold, R.S. Falk, and R. Winther. Finite element exterior calculus, homological techniques, and applications. *Acta Numerica*, pages 1–55, 2006.

[2] R. Barthelmé, P. Ciarlet Jr, and E. Sonnendrücker. Generalized formulations of Maxwell's equations for numerical Vlasov–Maxwell simulations. *Mathematical Models and Methods in Applied Sciences*, 17(05):657–680, 2007.

[3] R. Barthelmé and C. Parzani. Numerical charge conservation in particle-in-cell codes. *Numerical Methods for Hyperbolic and Kinetic Problems*, pages 7–28, 2005.

[4] D. Boffi. Compatible Discretizations for Eigenvalue Problems. In *Compatible Spatial Discretizations*, pages 121–142. Springer New York, New York, NY, 2006.

[5] D. Boffi. Finite element approximation of eigenvalue problems. *Acta Numerica*, 19:1–120, 2010.

[6] D. Boffi, F. Brezzi, and M. Fortin. *Mixed finite element methods and applications*, volume 44 of *Springer Series in Computational Mathematics*. Springer, 2013.

[7] J.P. Boris. Relativistic plasma simulations - optimization of a hybrid code. In *Proc. 4th Conf. Num. Sim. of Plasmas, (NRL Washington, Washington DC)*, pages 3–67, 1970.

[8] A. Bossavit. Solving Maxwell equations in a closed cavity, and the question of 'spurious modes'. *IEEE Transactions on Magnetics*, 26(2):702–705, March 1990.

[9] A. Buffa and I. Perugia. Discontinuous Galerkin Approximation of the Maxwell Eigenproblem. *SIAM Journal on Numerical Analysis*, 44(5):2198–2226, January 2006.

[10] M. Campos Pinto. Constructing exact sequences on non-conforming spaces. Submitted, 2015.

[11] M. Campos Pinto, S. Jund, S. Salmon, and E. Sonnendrücker. Charge conserving fem-pic schemes on general grids. *C.R. Mecanique*, 342(10-11):570–582, 2014.

[12] M. Campos Pinto and M. Mounier. Charge-conserving DG-PIC schemes on 2d cartesian meshes. In preparation.

[13] M. Campos Pinto and E. Sonnendrücker. Gauss-compatible Galerkin schemes for time-dependent Maxwell equations. http://hal.upmc.fr/hal-00969326, 2014.

[14] S. Caorsi, P. Fernandes, and M. Raffetto. On the convergence of Galerkin finite element approximations of electromagnetic eigenproblems. *SIAM Journal on Numerical Analysis*, 38(2):580–607 (electronic), 2000.

[15] B Bernardo Cockburn, George Karniadakis, and Chi-Wang Shu. *Discontinuous Galerkin methods : theory, computation, and applications*. Berlin ; New York : Springer, 2000.

[16] G. Cohen and P. Monk. Gauss point mass lumping schemes for Maxwell's equations. *Numerical Methods for Partial Differential Equations*, 14(1):63–88, 1998.

[17] M. Costabel and M. Dauge. Computation of resonance frequencies for Maxwell equations in non-smooth domains. In *Topics in computational wave propagation*, pages 125–161. Springer, Berlin, 2003.

[18] N. Crouseilles, P. Navaro, and E. Sonnendrücker. Charge conserving grid based methods for the Vlasov-Maxwell equations. *C. R. Mecanique*, 342(10-11):636–646, 2014.

[19] A. Dedner, F. Kemm, D. Kröner, C.-D. Munz, T. Schnitzer, and Wesenberg M. Hyperbolic divergence cleaning for the MHD equations. *J. Comput. Phys.*, 175:645–673, 2002.

[20] S. Depeyre and D. Issautier. A new constrained formulation of the Maxwell system. *Rairo-Mathematical Modelling and Numerical Analysis-Modelisation Mathematique Et Analyse Numerique*, 31(3):327–357, 1997.

[21] J.W. Eastwood. The virtual particle electromagnetic particle-mesh method. *Computer Physics Communications*, 64(2):252–266, 1991.

[22] J.W. Eastwood, W. Arter, NJ Brealey, and RW Hockney. Body-fitted electromagnetic PIC software for use on parallel computers. *Computer Physics Communications*, 87(1):155–178, 1995.

[23] T.Zh. Esirkepov. Exact charge conservation scheme for particle-in-cell simulation with an arbitrary form-factor. *Computer Physics Communications*, 135(2):144–153, 2001.

[24] L. Fezoui, S. Lanteri, S. Lohrengel, and S. Piperno. Convergence and stability of a discontinuous Galerkin time-domain method for the 3D heterogeneous Maxwell equations on unstructured meshes. *ESAIM: Mathematical Modelling and Numerical Analysis*, 39(6):1149–1176, November 2005.

[25] J.S. Hesthaven and T. Warburton. Nodal High-Order Methods on Unstructured Grids. *Journal of Computational Physics*, 181(1):186–221, September 2002.

[26] J.S. Hesthaven and T. Warburton. High-order nodal discontinuous Galerkin methods for the Maxwell eigenvalue problem. *Philosophical Transactions of the Royal Society A: Mathematical, Physical and Engineering Sciences*, 362(1816):493–524, March 2004.

[27] Didier Issautier, Frédéric Poupaud, Jean-Pierre Cioni, and Loula Fezoui. A 2-D Vlasov-Maxwell solver on unstructured meshes. In *Third international conference on mathematical and numerical aspects of wave propagation*, pages 355–371, 1995.

[28] A.B. Langdon. On enforcing Gauss' law in electromagnetic particle-in-cell codes. *Comput. Phys. Comm.*, 70:447–450, 1992.

[29] R. Leis. *Initial boundary value problems in mathematical physics*. John Wiley & Sons Ltd, 1986.

[30] P.J. Mardahl and J.P. Verboncoeur. Charge conservation in electromagnetic pic codes; spectral comparison of boris/dadi and langdon-marder methods. *Computer physics communications*, 106(3):219–229, 1997.

[31] B. Marder. A method for incorporating Gauss's law into electromagnetic PIC codes. *J. Comput. Phys.*, 68:48–55, 1987.

[32] P. Monk. An analysis of Nédélec's method for the spatial discretization of Maxwell's equations. *Journal of Computational and Applied Mathematics*, 47(1):101–121, 1993.

[33] Haksu Moon, Fernando L Teixeira, and Yuri A Omelchenko. Exact charge-conserving scatter–gather algorithm for particle-in-cell simulations on unstructured grids: A geometric perspective. *Computer Physics Communications*, 194:43–53, 2015.

[34] Marie Mounier. *Résolution des équations de Maxwell-Vlasov sur maillage cartésien non conforme 2D par un solveur Galerkin Discontinu.* PhD thesis, IRMA, université de Strasbourg, 2014. `https://tel.archives-ouvertes.fr/tel-01081560/`.

[35] C.-D. Munz, P. Omnes, R. Schneider, E. Sonnendrücker, and U. Voß. Divergence Correction Techniques for Maxwell Solvers Based on a Hyperbolic Model. *Journal of Computational Physics*, 161(2):484–511, July 2000.

[36] C.-D. Munz, R. Schneider, E. Sonnendrücker, and U. Voß. Maxwell's equations when the charge conservation is not satisfied. *Comptes Rendus de l'Académie des Sciences-Series I-Mathematics*, 328(5):431–436, 1999.

[37] J.-C. Nédélec. Mixed finite elements in $\mathbf{R^3}$. *Numerische Mathematik*, 35(3):315–341, 1980.

[38] R.N. Rieben, G.H. Rodrigue, and D.A. White. A high order mixed vector finite element method for solving the time dependent Maxwell equations on unstructured grids. *Journal of Computational Physics*, 204(2):490–519, April 2005.

[39] N.J. Sircombe and T.D. Arber. Valis: A split-conservative scheme for the relativistic 2d vlasov-maxwell system. *J. Comput. Phys.*, 228:4773–4788, 2009.

[40] A. Stock, J. Neudorfer, R. Schneider, C. Altmann, and C.-D. Munz. Investigation of the Purely Hyperbolic Maxwell System for Divergence Cleaning in Discontinuous Galerkin based Particle-In-Cell Methods. In *COUPLED PROBLEMS 2011 IV International Conference on Computational Methods for Coupled Problems in Science and Engineering*, 2011.

[41] T. Umeda, Y. Omura, T. Tominaga, and H. Matsumoto. A new charge conservation method in electromagnetic particle-in-cell simulations. *Computer Physics Communications*, 156(1):73–85, 2003.

[42] J. Villasenor and O. Buneman. Rigorous charge conservation for local electromagnetic field solvers. *Computer Physics Communications*, 69(2):306–316, 1992.

[43] K.S. Yee. Numerical solution of initial boundary value problems involving maxwell's equations in isotropic media. *IEEE Trans. Antennas Propag.*, 14(3):302–307, May 1966.

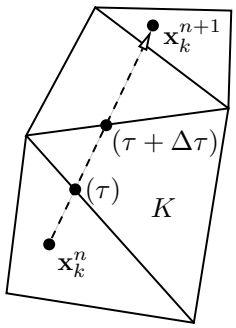

Figure 1: Charge-conserving current deposition on an unstructured grid

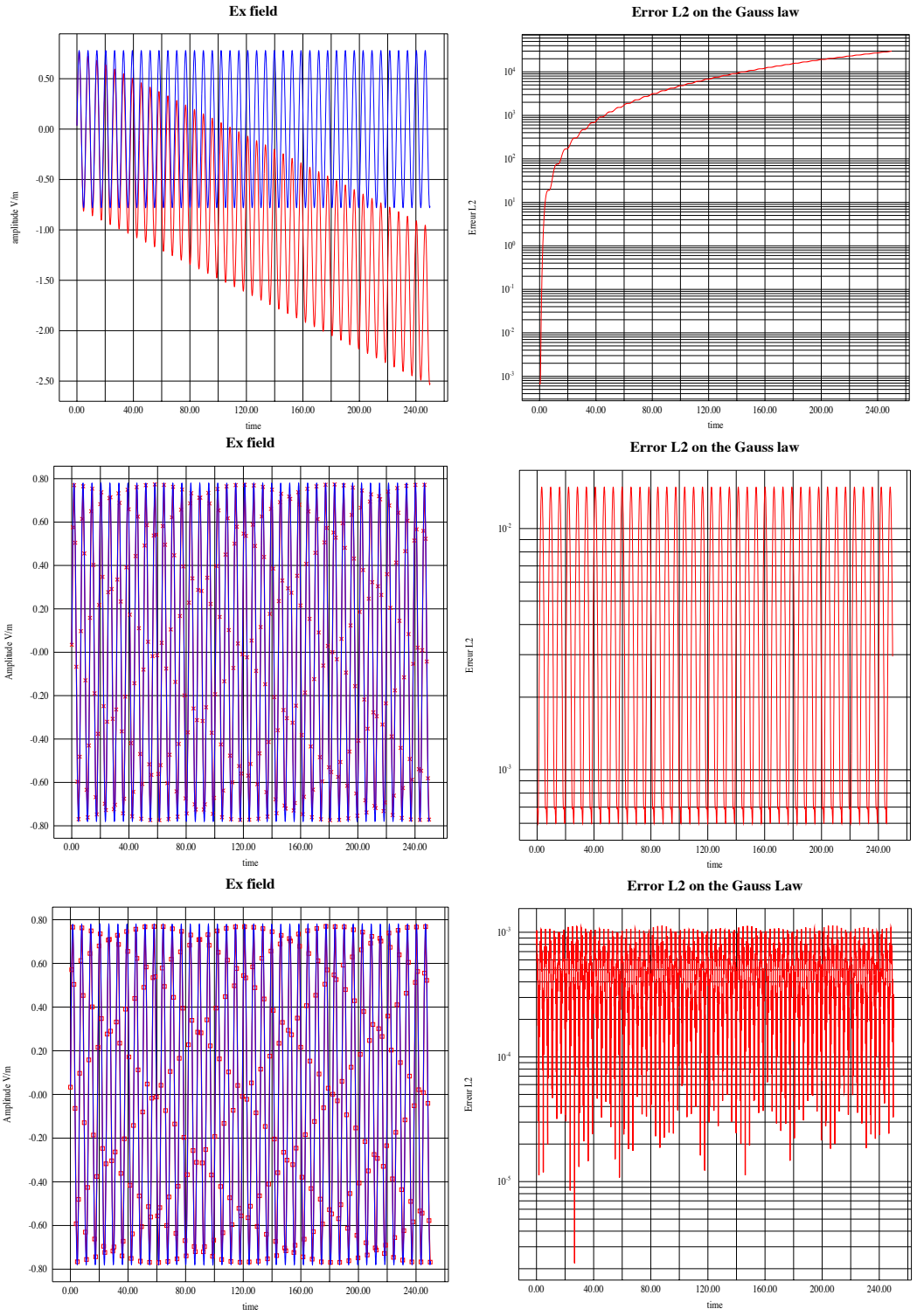

Figure 2: Depeyre-Issautier test case. On the left is shown the time evolution of E_x at a point for the exact solution (in blue) and the numerical ones (in red). The relative errors on the Gauss law are shown on the right. The rows correspond to different versions of a centered DG scheme (23) with $\mathbb{Q}_1$ elements on an 8×8 cartesian mesh: uncorrected (top), with hyperbolic field correction (center) and with source correction (bottom).

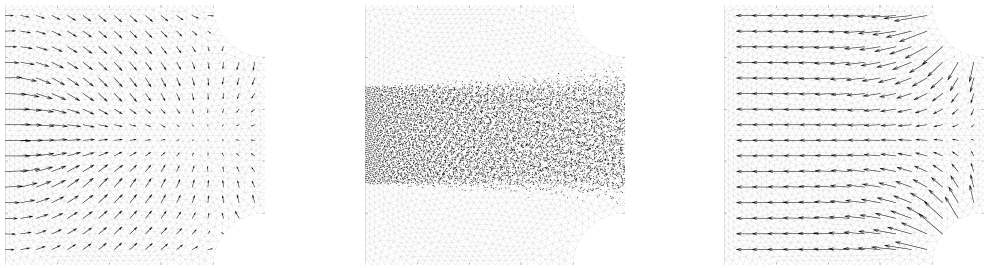

Figure 3: Beam test case. The self-consistent $\boldsymbol{E}$ field (left) and the numerical particles accelerated towards the right boundary (center) show the typical profile of the solution in the steady state regime. The external field $\boldsymbol{E}_{\text{ext}}$ is shown on the right panel.

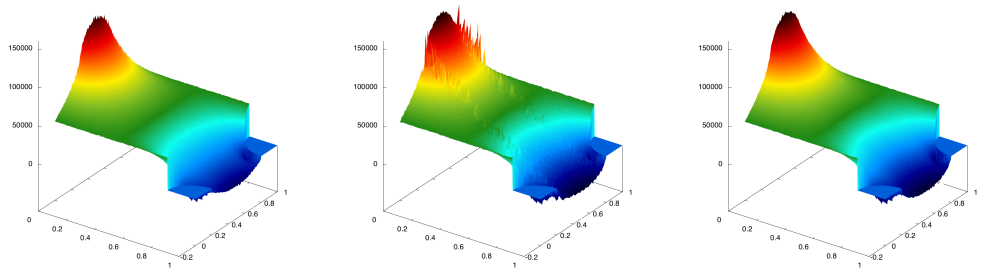

Figure 4: Beam test case. Snapshots of the self-consistent E_x field obtained with different schemes: a curl-conforming scheme with Nedelec elements $\mathcal{N}_{p-1}$ of maximal degree $p = 2$ (left) and a centered DG scheme with discontinuous elements of degree $p = 1$ using either a standard current deposition method (center) or a compatible current (right).

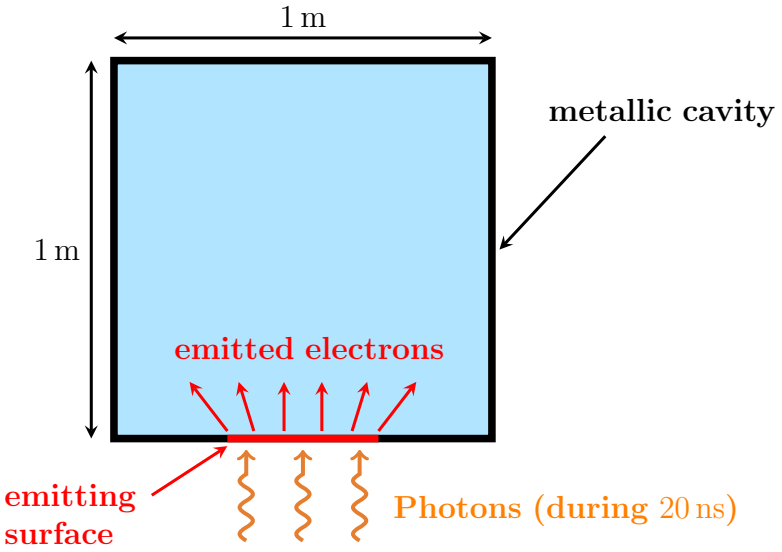

Figure 5: Illustration of the matter-photons interaction inside a metallic cavity.

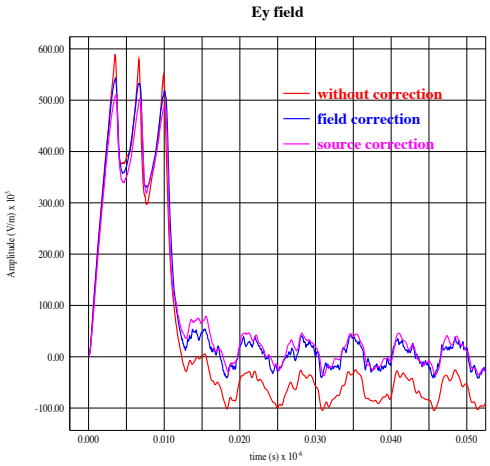

Figure 6: Matter-photons interaction inside a metallic cavity. Time evolution of the E_y field at a point $\mathbf{x} \approx (0, 0.5)$ in the emissive area obtained with three DGTD-PIC schemes (no correction, hyperbolic field correction and source correction).

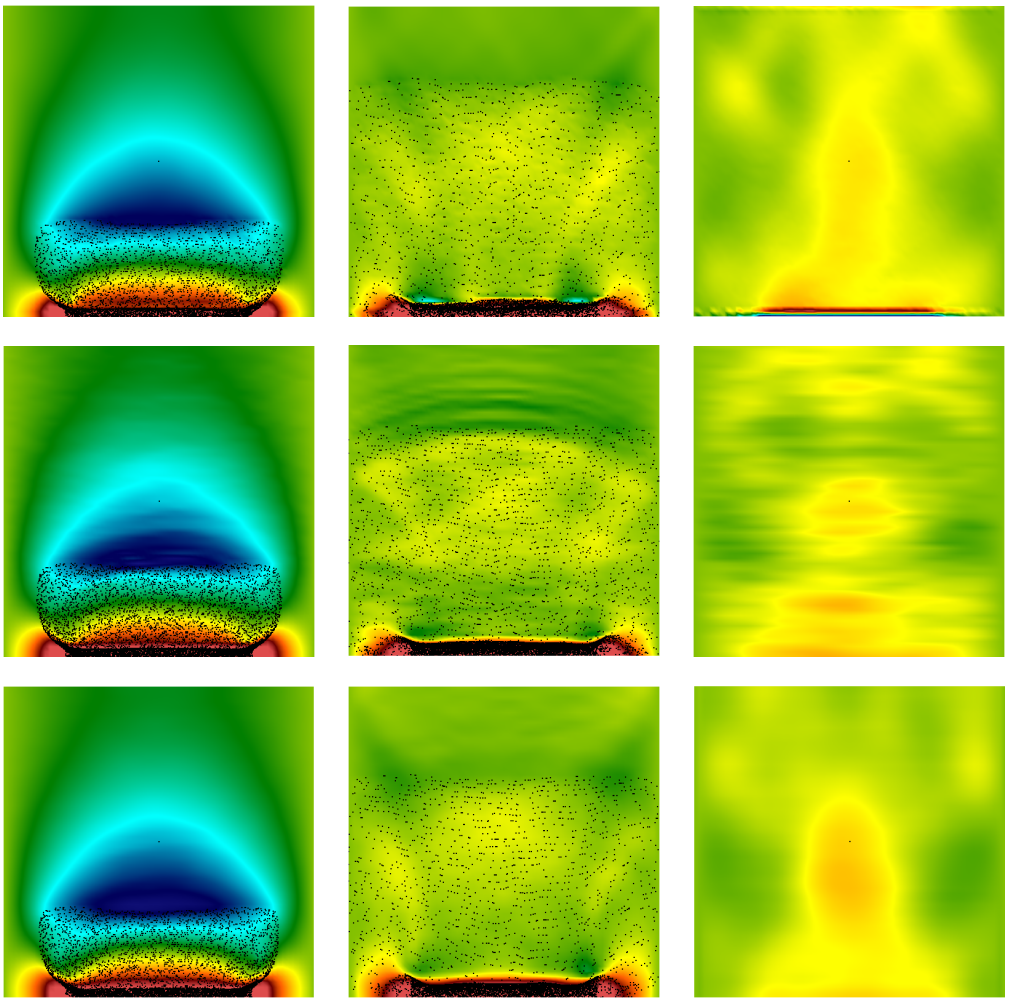

Figure 7: Matter-photons interaction inside a metallic cavity. Snapshots of E_y at $t = 5\,\text{ns}$ (left), $10\,\text{ns}$ (center) and $50\,\text{ns}$ (right) for three versions of the centered DG scheme (23) using $\mathbb{Q}_1$ elements on a 60×60 cartesian mesh. Top: uncorrected, center: with hyperbolic field correction, bottom: with source correction.

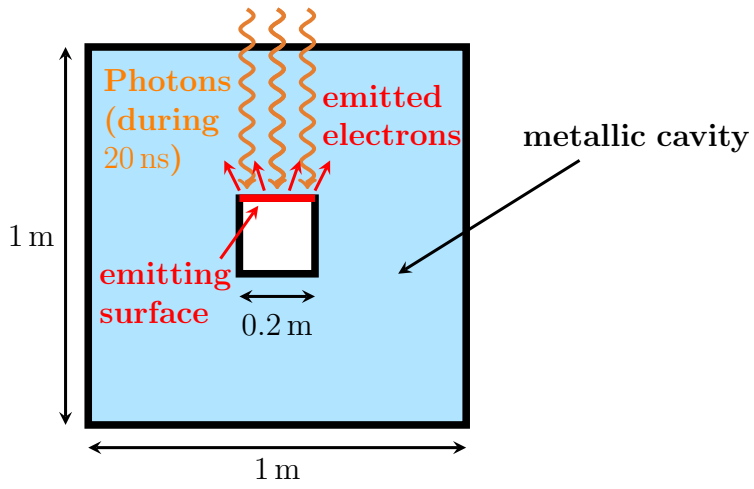

Figure 8: Illustration of the test-case of matter-photons interaction outside a metallic cavity

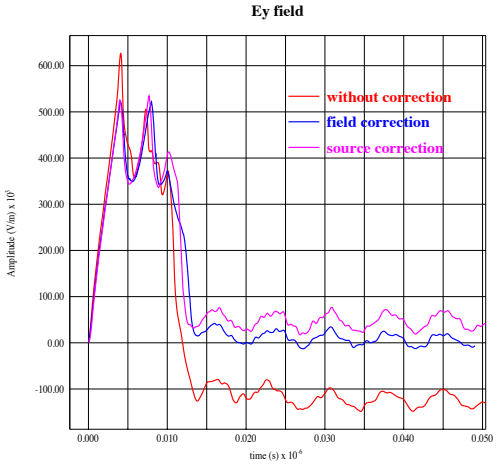

Figure 9: Matter-photons interaction outside a metallic object. Time evolution of the E_y field at a point $\mathbf{x} \approx (0, 0.1)$ in the emissive area obtained with three DGTD-PIC schemes (no correction, hyperbolic field correction and source correction).

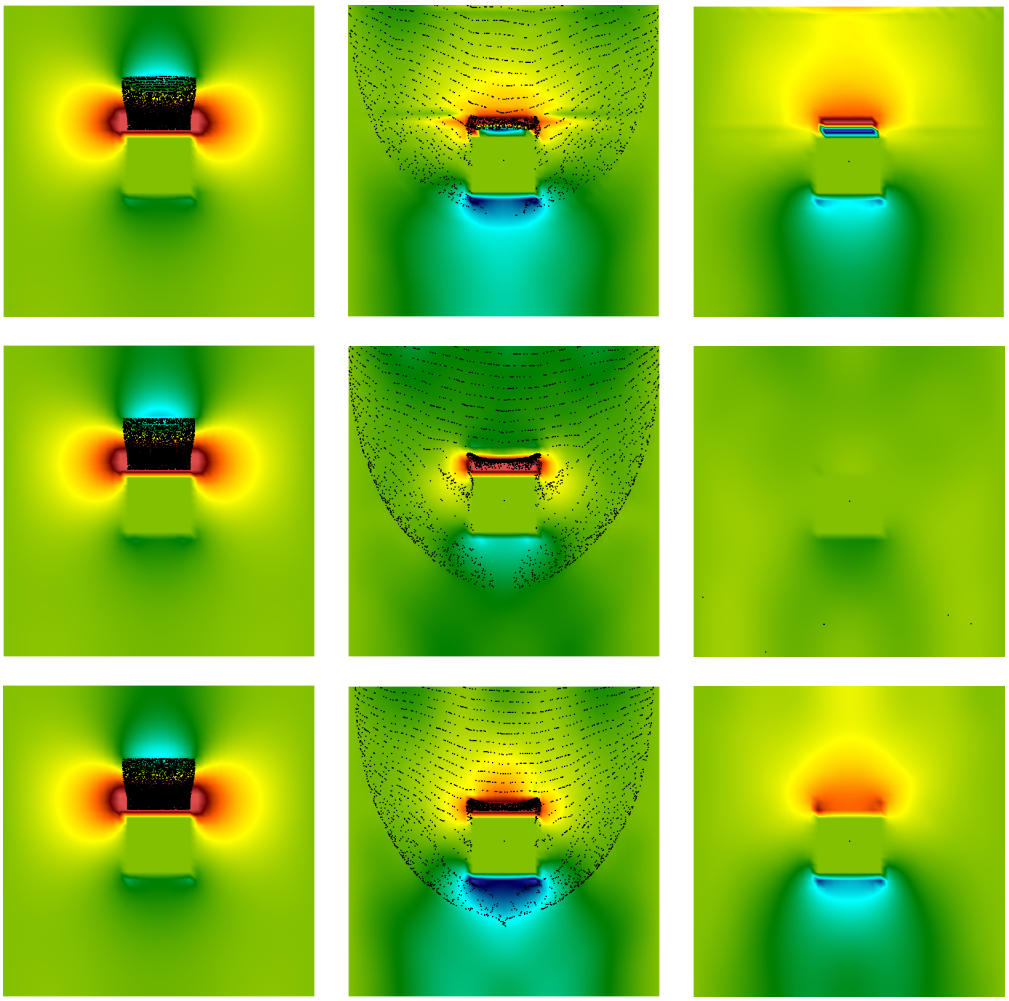

Figure 10: Matter-photons interaction outside a metallic object. Snapshots of E_y at $t = 5\,\text{ns}$ (left), $10\,\text{ns}$ (center) and $50\,\text{ns}$ (right) for three versions of the centered DG scheme (23) using $\mathbb{Q}_1$ elements on a 60×60 cartesian mesh. Top: uncorrected, center: with hyperbolic field correction, bottom: with source correction.